



**HAL**  
open science

## Morphodynamics of intertidal dune field in a mixed wave-tide environment: Case of Baie de Somme in Eastern English Channel

Imen Turki, Sophie Le Bot, Nicolas Lecoq, Hassan Shafiei, Charlotte Michel, Julien Deloffre, Arnaud Héquette, Vincent Sipka, Robert Lafite

### ► To cite this version:

Imen Turki, Sophie Le Bot, Nicolas Lecoq, Hassan Shafiei, Charlotte Michel, et al.. Morphodynamics of intertidal dune field in a mixed wave-tide environment: Case of Baie de Somme in Eastern English Channel. *Marine Geology*, 2021, 431, pp.106381. 10.1016/j.margeo.2020.106381 . hal-03041413

**HAL Id: hal-03041413**

**<https://hal.science/hal-03041413>**

Submitted on 2 Mar 2021

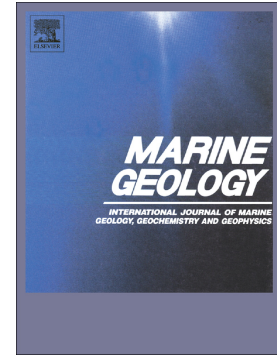
**HAL** is a multi-disciplinary open access archive for the deposit and dissemination of scientific research documents, whether they are published or not. The documents may come from teaching and research institutions in France or abroad, or from public or private research centers.

L'archive ouverte pluridisciplinaire **HAL**, est destinée au dépôt et à la diffusion de documents scientifiques de niveau recherche, publiés ou non, émanant des établissements d'enseignement et de recherche français ou étrangers, des laboratoires publics ou privés.

## Journal Pre-proof

Morphodynamics of intertidal dune field in a mixed wave-tide environment: Case of Baie de Somme in Eastern English Channel

Imen Turki, Sophie L.E. Bot, Nicolas Lecoq, Hassan Shafiei, Charlotte Michel, Deloffre Julien, Arnaud Héquette, Vincent Sipka, Lafite Robert



PII: S0025-3227(20)30269-3

DOI: <https://doi.org/10.1016/j.margeo.2020.106381>

Reference: MARGO 106381

To appear in: *Marine Geology*

Received date: 10 July 2019

Revised date: 22 September 2020

Accepted date: 14 November 2020

Please cite this article as: I. Turki, S.L.E. Bot, N. Lecoq, et al., Morphodynamics of intertidal dune field in a mixed wave-tide environment: Case of Baie de Somme in Eastern English Channel, *Marine Geology* (2018), <https://doi.org/10.1016/j.margeo.2020.106381>

This is a PDF file of an article that has undergone enhancements after acceptance, such as the addition of a cover page and metadata, and formatting for readability, but it is not yet the definitive version of record. This version will undergo additional copyediting, typesetting and review before it is published in its final form, but we are providing this version to give early visibility of the article. Please note that, during the production process, errors may be discovered which could affect the content, and all legal disclaimers that apply to the journal pertain.

© 2018 Published by Elsevier.

# **Morphodynamics of intertidal dune field in a mixed wave-tide environment: case of Baie de Somme in Eastern English Channel**

**Imen TURKI<sup>1\*</sup>, Sophie LE BOT<sup>1</sup>, Nicolas LECOQ<sup>1</sup>, Hassan SHAFIEI<sup>2</sup>, Charlotte MICHEL<sup>1</sup>, Deloffre Julien<sup>1</sup>, Arnaud Héquette<sup>3</sup>, Vincent Sipka<sup>3</sup>, Lafite Robert<sup>1</sup>**

<sup>1</sup> Continental and Coastal Morphodynamic Laboratory, Normandie University, UNIROUEN, UNICAEN, CNRS UMR 6143, M2C, 76000 Rouen.

<sup>2</sup> LEGI, UMR CNRS 5519, Grenoble Alpes University, 11 rue des Mathématiques (BP46), 38058, Grenoble, France 5519

<sup>4</sup> Laboratoire d'Océanologie et de Géosciences, University Littoral Côte d'Opale, Univ. Lille, CNRS, UMR 8187, LOG, 62930 Wimereux, France

\* Corresponding Author: imen.turki@univ-rouen.fr

## Abstract

Understanding the response of the intertidal dunes to the varying hydrodynamic conditions in mixed wave-tide environments is of high complexity. Field measurement is one of the most useful approaches to investigate the dune dynamics at different time (semi-diurnal and lunar cycles) and spatial (dunes and associated superimposed bedforms) scales. High-resolution laser scanner data for five successive surveys over a full neap-spring cycle (27 January – 9 February 2014), together with hydrodynamic measurements, have been explored to investigate the morphodynamics of dunes, their superimposed bed forms and their migration in a mixed wave-tide environment (case of the Baie de Somme Eastern of the English Channel), by the use of a stochastic-physical coupling approach. The dunes are  $\sim 12$  m wavelength, 0.4 height and oriented orthogonally to the shoreline with angles varying between  $-45^\circ$  and  $+45^\circ$  corresponding to clockwise and counter-clockwise changes, respectively.

A stochastic approach, based on spectral analysis, exhibits a series of morphological defects modulating the dune changes following several scale ranges in response to various energy conditions. Such defects can be classified into four categories: (1) limited structures of  $\sim 1.6$  m wavelengths locally developed along the dune during flood drainage; (2) small-scale superimposed bedforms of  $\sim 3.2$  m wavelengths built-up across the dunes after high hydrodynamics and proliferated when the energy decreases; (3) large-scale superimposed bedforms of  $\sim 6.4$  m resulting from the morphological growth of the smaller bedforms; (4) crestline sinuosity with  $\sim 25$  m wavelength and induced by changes in the orientation of the dunes when they are exposed to high tide-wave activity. The evolving dune defects over the neap-spring cycle is strongly related to the physical mechanisms of sediment transport supplying the migrating dunes and favourable for their self-organization.

The physical study of the migrating dunes with the wave-tide driven sediment transport highlights that the long-dune migration components are significantly important during high-energy episodes with a mean explained variance of 65% of the total migration while they decrease to 32% for moderate wave-tide conditions. Good matches of the cross- and long-migration components with the along-shore and the cross-shore sediment transport quantities are recorded with  $R^2$  coefficients higher than 70%. These coefficients increase for the offshore dunes where their morphological response to the time-averaged sediment transport is faster while onshore dunes respond at slower timescales resulting in lower  $R^2$  coefficients.

**Keywords:** stochastic-physical coupling approach, dune morphodynamics, morphological defects, superimposed bedforms, crestline sinuosity, dune migration, wave-tide driven sediment transport.

## 1. Introduction

The exposure of the coastal zones to flooding hazards is generally influenced by a series of physical factors including the changes in the wave energy conditions, the tidal currents and the morphology of the coastal environments including man-made structures, as well as the sea-level rise impact (e.g. Priest and Allan, 2004). Accurate investigation on the multiscale natural responses of the coastal sedimentary structures to the hydrodynamic forces and the potential impacts of the human-induced climate change is strongly required to improve our knowledge of coastal risks. A deep understanding of the morphology evolution and migration of bedforms at small scales is crucial to forecast larger coastal responses (e.g. Boyd et al., 1992; Komar et al., 1999; Stockdon et al., 2006).

Coastal bedforms are considered as one of the most influential nearshore features. Their evolution depends on the combining effects of tides, winds, waves, and their associated currents, which are responsible for some dramatic changes in the coastal morphology. Dunes

are common patterns appearing ubiquitously in natural aeolian (e.g. Charru et al., 2013), fluvial (e.g. Parsons et al., 2005) and submarine environments (e.g. Zhou et al., 2020) and changing under oscillatory flows at multiple spatial and temporal scales. In marine environments, subaqueous dunes occur in both subtidal (e.g. Ferret et al., 2010; Van Landeghem et al., 2012) and intertidal (e.g. Masselink et al., 2009) environments. They are formed and controlled by coastal sediment dynamics and interactively influence it as well in environments where the key role of the tidal forcing is dominant with the additional effects of waves.

Considerable efforts have been invested by the use of different approaches to improve the understanding of the physical processes responsible for the morphological changes of subaqueous dunes at various scales of time and space. Numerous researchers have used experimental tests in laboratory flumes with unidirectional, steady and uniform currents (e.g. Bennett and Best, 1995; Best and Kostaschuk, 2002; McLean et al., 1994; Vah et al., 2020) to develop empirical relationships between dunes and their controlling environmental variables. Furthermore, various studies have investigated the dune dynamics either: (1) for determining the transport regimes and the depth-scaling rules (e.g. Cheng et al., 2004; Villard and Church, 2005; Bartholdy et al., 2005, 2008), or (2) for exploring the relationship between the field dune migration rates and the empirical/numerical bedload transport rates (e.g. Hoekstra et al., 2004; Kostaschuk et al., 2004; Masselink et al., 2009; Williams et al., 2006; Vah et al., 2020). Because of the difficulties for determining the net sediment transport in coastal environments, few studies have been conducted using field sedimentary measurements over an extended period of time (e.g., Gonzalez and Eberli, 1997; Whitmeyer and FitzGerald, 2008) to gain insight into the net sediment transport patterns and the associated morphological developments.

The morphological evolution of dunes is mainly controlled by changes in the hydrodynamic energy conditions (e.g. Wilbers, 2004; Wilbers and ten Brinke, 2003). Indeed, the morphological tracking of dunes as a response to climate-driven forces (such as wave, wind, and tides) has been carried out by several works using field observations (e.g. Masselink et al., 2009), laboratory experiments (e.g. Venditti et al., 2005; Fernandez et al., 2006) and numerical modelling (e.g. Pattanapol et al., 2008; 2011; Wakes et al., 2010).

Small-scale superimposed bedforms are frequently observed over dunes (e.g. Galeazzi et al., 2018). Their morphodynamics is studied by Venditti et al. (2005) and Fernandez et al. (2006) using data drawn by laboratory experiments. Venditti et al. (2005) have shown that the height of the sand sheets superimposed over the dunes is 0.1 times the height of the dunes themselves while the superimposed bedforms migrate 8 to 10 times faster than the dunes with nearly constant lengths under similar flow conditions inducing the migration of the larger dunes.

Considerable efforts have been invested in understanding the physical processes leading to the growth of the morphological patterns and predicting their characteristics (e.g. Huntley et al., 2008; Williams et al., 2005). As reported in these works, the response of seabed characteristics to hydrodynamic-driven forces is strongly influenced by the presence of some morphological irregularities, which can be described by the term 'defect'. The pioneering work of Huntley et al. (2008) highlighted the key role that the dynamics of these defects play in the development of the morphological bedforms as a response to changes in energy activity.

Complex-system approaches have been applied to different geomorphological environments and have proven to be helpful for investigating the morphological changes at several time-scales and identifying the relation between the large- and the small-scale dynamics of morphological patterns (e.g., Werner and Kocurek, 1997; Werner, 1999). For example,

Werner and Kocurek (1997) works showed the physical control exerted by the morphological large-scale pattern dynamics (e.g. change in relief and migration of patterns) on the morphological small-scale dynamics (e.g. sea bed roughness, and small defects).

Then, alternative approaches were developed from the studies of the nonlinear systems, including deterministic chaos, self-organization, and emergent phenomena (e.g. Falques et al., 2000; Asthon et al., 2001; Murray and Thieller., 2004). Murray et al. (2014) studied the stochastic behavior of the autogenic changes in a morphological system's configuration. They demonstrated that these changes could be highly pronounced, leaving complex signatures behind, and could be mistaken with other changes occurring within the system (e.g. changes in forcing, boundary conditions and threshold-like responses to gradual changes).

However, investigations focusing on the spatial and temporal process-response relationships of a dune field with the hydrodynamics, including the morphological changes of the migrating dunes and their superimposed bedforms, are limited. Overall, the evolution of the intertidal dune fields in coastal areas over neap-spring cycles and under fluctuating wave-tide driven forces remains underexplored (e.g. Hellestra et al., 2004).

This work focuses on the dynamics (i.e. morphological changes and migration) of an intertidal dune field in relation with the hydrodynamic interactions of wave-tide driven forces in a coastal-estuarine environment by the use of a stochastic-physical coupling approach. Here, we gain insight into a series of subaqueous dune surveys, located along the intertidal area of the Baie de Somme (NW France, English Channel), to investigate the multiscale variability of the dunes, their morphological defects and their migration in response to wave-tide conditions during a full neap-spring tidal cycle.

## **2. Methodological Approach**

### ***2.1 Dune fields in the Baie de Somme***

The Baie de Somme is an hypertidal bay of the eastern English Channel (NW France) (Fig. 1). As documented by Michel et al. (2017), the intertidal sandy area of the bay of 42.5 km<sup>2</sup> is covered by more than 4 000 hydraulic dunes with different sizes. The mean height, wavelength and sinuosity of the dunes are 0.375 m (s.d. 0.25), 17.7 m (s.d. 9.9) and 0.958 (s.d. 0.08).

The bay is classified as a mixed wave-tide dominated estuary (Michel et al., 2017). It is fed by two rivers with small mean flow rates of around 1.5 m<sup>3</sup>/s for the Maye river and 32 m<sup>3</sup>/s for the Somme river. This latter is channeled and equipped with locks (Bellesort and Migniot, 1987; Loquet et al., 2000), which explain the bay does not function as an estuary anymore. The study area is characterized by semi-diurnal tides ranging between 8.5 m and up to 10.5 m at mean spring conditions and during exceptional spring tides, respectively. The bay is exposed to swell waves coming from West for 75% of the time with the mean significant offshore wave height and period of around 2 m and 7 s, respectively (Bellesort and Migniot, 1986). When offshore waves enter the bay, some 6 km west of the study area in the vicinity of the lowest astronomical tides, they are damped when passing over the sedimentary bulge of the ebb delta and then progress on the dissipative sandy foreshore (Fig. 1).

The present study focuses on an intertidal dune field (50°13.178'N, 1°33.569'E), sloped with 3 % and located some hundreds of meters off the coastline, oriented WSW-NE (Fig. 1). The dunes correspond to medium to large dunes with a mean height and wavelength of 0.371 m (s.d. 0.07) and 12.71 m (s.d. 2.46), composed of fine to medium sand with a D<sub>50</sub> of 0,220 mm.

The characteristics of dunes in this area are similar to those observed in the whole bay (e.g. dune height and length, sediment grain size) and can hence be considered as representative of the dunes observed in the whole bay. The mean sinuosity is between 0.07 and 2.46.

*Fig.1 Distribution of intertidal dunes (blue lines) in the Baie de Somme (NW France) and location of the study area (black rectangle). Topography was obtained from aerial LIDAR (aircraft) data collected on 1<sup>st</sup> April 2013. White areas correspond to the main under water tidal channels which are not covered with laser topographic data.*

## **2.2. Topographic measurements**

Five topographic surveys (from  $S_1$  to  $S_5$ ) were carried out during a full neap-spring tidal cycle of 24 tidal cycles (from  $T_1$  to  $T_{24}$ ) over the winter period of January-February 2014. They were carried out approximately every 3 days from 27<sup>th</sup> January 2014 to 09<sup>th</sup> February 2014 (Michel, 2016), after tides  $T_2$ ,  $T_6$ ,  $T_{13}$ ,  $T_{19}$ , and  $T_{24}$ . The topographic measurements were conducted within an area of 2500 m<sup>2</sup> using a terrestrial laser scanner (TLS; Leica Scan Station C10, © Leica Geosystems) with an accuracy comprised between 2 and 3 cm and an horizontal resolution varying between several millimeters to some centimeters depending on the survey. Digital Elevation Models (DEMs) were produced with a 10-cm horizontal resolution (Fig.2a). Topographic information in each cell corresponds to the mean topographic value calculated from the TLS measurements, given in the IGN69 French altitude referencing system. In order to quantify the morphological changes, dune tracking was conducted on four lines (A, B, C and D) on a series of six medium to large dunes ( $DF_1$  to  $DF_6$ ) (Fig. 2a). The lines are orthogonal to the full dunes (parallel to the shoreline position) and 20 m spaced. This allows the identification of 24 dune sections in the field for each survey ( $D_1$  to  $D_{24}$ ; Fig. 2a). The

dunes are North-South elongated, almost orthogonal to the shoreline. The mean orientation of dunes and their crestlines are also identified.

Over the dunes, a complex topographic pattern is observed showing a series of irregularities, mainly parallel to x-axis, with different ranges of scales, smaller than the mean dune wavelength ( $\sim 12$  m), as illustrated in Fig. 2b, 2c and 2d. The smallest bedforms (ripples), with wavelengths of some tens of centimetres, visible on the field photography (Fig. 2d), can not be detected from the topographic data, given the DEM resolution (10 cm).

As illustrated in Fig.3a, the number of dunes in the field is conserved between the different surveys (6 full dunes and 24 dune sections). In the present work, we consider each dune section (D) as individual, independent from the neighbor sections, although belonging to the same full dune (DF). Then, the morphological changes of D (a part of DF) are also considered independent. Changes in the bed elevations of the dune field have been calculated between two successive TLS; they are presented in Fig3b as a digital elevation models of difference (DoDs) for the different time intervals ( $I_1$  to  $I_4$ ). The DoDs have been used in the present work for tracking the morphological changes of dunes and quantifying the different categories of defects according to their length of scales.

We designate the wavelength and the angle of dunes by, respectively,  $\lambda_d$  and  $\gamma_b$  with respect to the y-axis (orthogonal to the shoreline, North oriented). Both characteristics have been measured from the DEM associated to the different surveys ( $S_1$  to  $S_5$ ) for all dune sections (from  $D_1$  to  $D_{24}$ ).

*Fig. 2. Topography of the dune field offshore Le Hourdel (Baie de Somme). See location on Fig. 1. (a) Digital Elevation Model (DEM) of the intertidal dune field provided by a terrestrial laser scanner (survey S1; 28<sup>th</sup> January 2014); z-axis is the bed level with respect to the IGN69 French referencing system; x- and y- axes are parallel and perpendicular to the shoreline orientation respectively. Dashed lines underline the orientation of the dune portions D1 to D24 and surveyed along the*

different lines A, B, C, and D. The white and the grey circles represent the position of the ADCP instruments North « Up » and South « Down » respectively. (b) Zoom on the topography of dunes DF3 to DF5 (survey S1; 28th January 2014) illustrating the complex topographic pattern including defects (bedforms, sinuosity). Examples of morphological defects, with different wavelengths and orientations, are presented by red arrows. (c) Topographic section along the profile B extracted from the DEM, measured on 28th January 2014, orthogonally to dunes. Examples of morphological defects are presented by red arrows. (d) Photography of dunes DF2, DF3 and DF4 the 28th Jan 2014.

Fig.3 (a) Topography of the dune field for the different surveys and changes in the time intervals. a) Digital elevation models (DEMs); b) Digital elevation models of difference (DoDs). Surveys are named S1 (28th January 2014), S2 (30th January 2014), S3 (3th February 2014), S4 (6th February 2014), and S5 (9th February 2014). (b) Topographic changes in the study dune field during the period on 27th January 2014 to 09th February 2014 for the I1 (between S2 and S1), I2 (between S3 and S2), I3 (between S4 and S3) and I4 (between S5 and S4) time intervals. The color scale represents the level variation  $\Delta z$ .

### **2.3 Hydrodynamic observations and estimation of sediment transport**

The driving forces of the nearshore hydrodynamic conditions were determined from various observations during a neap-spring cycle of 24 tides from 27<sup>th</sup> January 2014 to 9<sup>th</sup> February 2014. Hydrodynamic measurements were carried out by the means of two ADCP profilers (1228 kHz, Sentinel, ©Teledyne RDI), located within the study area (50° 13.178'N, 1° 33.569'E; Fig. 2), spaced 40 m and both positioned in a dune trough at the beginning of the survey: the first ADCP is located in the North of the dune field (grey circle in Fig.2.a) and was faced up to record data above the altitude of 2.4 m IGN69 (from 0.7 m above the seabed, at the beginning of the survey, up to the sea surface) ; the second one, located in the southern

part (white circle in Fig.2.a), was faced down to record data from the seabed up to 0.5 to 1.2 m, depending on dune crest and trough positions varying in response to dune migration during the whole neap-spring tidal cycle. Cell sizes are 0.1 and 0.2 m respectively for the South (down-looking) and North (up-looking) ADCPs. ADCP measurements have been merged to provide information on the whole water column, from the northern ADCP for the upper part (above the altitude 2.4m IGN69) and from the southern one for the lower part (beneath the altitude 2.4m IGN69). ADCPs provide data on: (i) magnitude and direction of currents which correspond to the mean values obtained every 1 minute from 2 Hz measurements (burst mode), and (ii) wave direction and wave significant height, extracted from ADCP data using WavesMon software (©Teledyne RDI), corresponding to the mean values at the scale of the burst (every one minute). ADCP data have been further used to calculate waves and currents at the sea surface and 1 m above the seabed (i.e. several tens of centimeters above the dunes of around 0.3 m height) (Fig.4).

*Fig. 4. Hydrodynamic measurements in the dune field of the Baie de Somme during the 24 tides from 27<sup>th</sup> January and 8<sup>th</sup> February 2014: (a) water depth; 1 m above the bottom (red) and the sea-surface (blue) current velocities (b) and directions (c); (d) wave height; (e) wave direction. The averaged directions (currents, waves) during each tidal cycle is also represented (arrows).*

Sediment transport quantities were empirically computed for each dune section (from D<sub>1</sub> to D<sub>24</sub>) between two successive surveys (time intervals I<sub>1</sub>, I<sub>2</sub>, I<sub>3</sub> and I<sub>4</sub> respectively between surveys S<sub>1</sub> to S<sub>5</sub>). The time-averaged transport rate of the bedload and the suspended sediment transport  $\overline{q_t}$  was calculated based on Bailard (1981) energy equation:

$$\langle \overline{q_t} \rangle = \overline{q_b} + \overline{q_s} = \rho C_f \frac{\varepsilon_b}{\tan \phi} \left[ \langle |v_b|^2 \vec{v} \rangle - \frac{\tan \beta}{\tan \phi} \langle |v_b|^3 \vec{i} \rangle \right] + \rho C_f \frac{\varepsilon_s}{w_s} \left[ \langle |v_s|^3 \vec{v} \rangle - \frac{\varepsilon_s}{w_s} \tan \beta \langle |v_s|^5 \vec{i} \rangle \right] \quad (1)$$

the subscripts ‘b’ and ‘s’ indicate, respectively, the bedload and suspended sediments;  $C_f$  is the friction coefficient;  $w_s$  is the sediment fall velocity;  $\varepsilon_b$  and  $\varepsilon_s$  are the bedload and suspension efficiency factor;  $\phi$  is the internal angle of friction;  $\tan \beta$  is the bed slope of the dune field;  $\vec{i}$  is the unit vector in the down-slope direction;  $v_b$  and  $v_s$  are the velocities resulting from the currents and waves at 1 m above the bottom and the sea surface.

Here, the dispersion equation (Eq.2) has been used to determine the velocity  $v$  considering the wave-current interaction described by the angle of waves travelling in the presence of currents  $\alpha$ .

$$(w - v \cdot k \cdot \cos \alpha)^2 = g \cdot k \cdot \tanh(kh) \quad (2)$$

where  $w$  is the wave radian frequency,  $k$  is the wavenumber, and  $h$  is the water depth. We have  $\alpha = 0 \text{ rad}$  when currents travel in the same direction as waves, and  $\alpha = \pi \text{ rad}$  for currents in the opposite direction to that of waves.

$v_b$  and  $v_s$  have been calculated by the use of  $\alpha_b$  (angle between waves and currents 1 m above the bedload) and  $\alpha_s$  (angle between the waves and sea surface currents), respectively.

The total transport  $q_t$  is decomposed into both longshore and cross-shore directions since the velocity norm  $v$  can be defined as  $\sqrt{U^2 + V^2}$ ; for simplifications,  $\beta$  is zero under the assumption of non-significant cross-shore and longshore bed gradients; We call  $U_b$  ( $U_s$ ) and  $V_b$  ( $V_s$ ) are the components in  $X$  and  $Y$  directions respectively at 1 m above the bottom (at sea surface).

The two time-averaged cross-shore (with *cs*h subscript) and longshore (with *lsh* subscript) components of sediment transport rates are expressed as the following:

$$\langle q_{lsh} \rangle = \rho C_f \frac{\varepsilon_b}{\tan \phi} \left[ \sqrt{U_b^2 + V_b^2} U_b \right] + \rho C_f \frac{\varepsilon_s}{w_s} \left[ \sqrt{U_s^2 + V_s^2} U_s \right] \quad (3)$$

$$\langle q_{csh} \rangle = \rho C_f \frac{\varepsilon_b}{\tan \phi} \left[ \sqrt{U_b^2 + V_b^2} V_b \right] + \rho C_f \frac{\varepsilon_s}{w_s} \left[ \sqrt{U_s^2 + V_s^2} V_s \right] \quad (4)$$

By assuming the bed gradient to zero in the study area (bed slope is of 3%), the gravitational transport terms are dropped from Eq.3 and Eq.4.

With the aim of calculating the sediment transport components with respect to the dune orientation, we consider an angle  $\gamma_b$  between the dune crestline and the normal to the shoreline (Fig.5.a):  $\gamma_b$  takes a value of zero for dunes fully orthogonal to the shoreline.  $\gamma_b$  was determined for each dune section and was used to calculate the cross-dune ( $q_{cd}$ ) and the long-dune ( $q_{ld}$ ) direction transport :

$$q_{cd} = q_{lsh} \cos \gamma_d - q_{csh} \sin \gamma_d \quad (5)$$

$$q_{ld} = q_{lsh} \sin \gamma_d + q_{csh} \cos \gamma_d \quad (6)$$

The components  $q_{cd}$  and  $q_{ld}$  were empirically computed with the same time resolution of the measured data (i.e. 1-minute measurements) and then integrated into the space (along the dune section) and the time (over the time elapsed between two successive surveys) domains to define finally the two transport components, i.e.  $q_{cd}$  and  $q_{ld}$ , for each dune section and each morphological survey.

*Fig. 5 Parametrization of dune migration process. (a) Determination of the dune angle  $\gamma$  between its crestline and the orthogonal to the shoreline. Approximation approach to calculate: (b) the local gradient of dune variation between two positions  $X_{n-1}$  and  $X_{n+1}$ ; (c) the dune movement  $\vec{M}$ , between  $t_i$  and  $t_{i+1}$ , which is decomposed in the directions  $X$  and  $Y$ .  $\vec{M}$  is the mean between  $D_{n-1}$  to  $D_{n+1}$  and is described as the components  $M_x$  (orthogonal to the dune crest) and  $M_y$  (parallel to the dune crest).*

The constant values used in this simulation are:  $C_f = 0.03$ ;  $\varepsilon_b = 0.21$ , and  $\varepsilon_s = 0.025$  for the longshore transport;  $\varepsilon_b = 0.1$ , and  $\varepsilon_s = 0.02$  for the cross-shore transport (Bailard, 1981; Bailard and Inman, 1981);  $w_s$  values, calculated from the granulometric data from the dune field seabed, are  $2.8 \cdot 10^{-3} \text{ ms}^{-1}$  and  $1.35 \cdot 10^{-3} \text{ ms}^{-1}$  for the bedload and the suspended sediment transport respectively (Soulsby, 1997);  $\tan\phi = 0.63$ ;  $\tan\beta = 0$ ;  $\rho_s = 2650 \text{ kgm}^{-3}$ ;  $\rho = 1000 \text{ kgm}^{-3}$ ;  $g = 9.8 \text{ ms}^{-2}$ ; and  $p = 0.3$ .

In order to investigate the effects of waves on the dune changes, the components of cross- and long-dune energy have been quantified. Similar to  $q_{csh}$  and  $q_{lsh}$ ,  $EF_{cd}$  and  $EF_{ld}$  are expressed as:

$$EF_{cd} = EF_{lsh} \cos \gamma d - EF_{csh} \sin \gamma d \quad (7)$$

$$EF_{ld} = EF_{lsh} \sin \gamma d + EF_{csh} \cos \gamma d \quad (8)$$

Where  $EF_{csh}$  and  $EF_{lsh}$  represent the cross-shore and the long-shore components of the energy flux EF respectively. They are expressed as  $EF_{csh} = EF \cdot \cos \theta$  and  $EF_{lsh} = EF \cdot \sin \theta$ .

$\theta$  is the wave angle with respect to the shoreline position;  $EF = E \cdot C_g$ ;  $C_g$  is the group celerity, and  $E$  is the total wave energy based on the significant wave height ( $E = \frac{1}{8} \cdot \rho \cdot g \cdot H_s^2$ ).

The energy flux components, i.e.  $EF_{cd}$  and  $EF_{ld}$ , have been calculated for each tide ( $T_1$  to  $T_{25}$ ) by integrating the 1-minute measurements during a full tidal cycle.

#### ***2.4 Spectral analysis for morphological decomposition at different spatial scales using continuous wavelet transform***

Dunes present a complex morphological pattern, induced by the presence of defects (superimposed bedforms, dune sinuosity). As well, changes in dune morphology are very

complex (Fig. 3). This evolving variability is considered as non-linear, in response to the hydrodynamic conditions and the resulting dune and defects migration, and results from a combination of several morphological modulations at various ranges of scale. Decomposing this variability into different frequencies is required to identify the sedimentary structures of migrating dunes and improve our understanding of their organization under fluctuating conditions of energy and sediment transport.

The Continuous Wavelet Transform (CWT) has been largely used in meteorological applications to investigate the time frequency evolution of the climate patterns (e.g., Turki et al., 2015; Massei et al., 2017). Such analyses are widely documented in the literature (e.g. Labat, 2005). The technique of wavelet consists of decomposing a variability signal into scaled and translated versions (i.e. daughter wavelets) of a reference wave function (i.e. mother wavelet). The correlation between the undecomposed signal and the larger daughter wavelets allows the identification of different scales of the variability. For example, the existence of a correlation between the undecomposed signal and the smaller wavelets emphasizes the presence of the smaller (shorter wavelengths) variations in the undecomposed signal. Scanning the undecomposed signal with the set of daughter wavelets (i.e. convolving the signal with the wavelets) produces a diagram of space (X direction) versus space frequency of the variability.

In the present study, the stochastic approach of CWT has been applied to changes in bed elevation (DoDs, Fig. 3b) to inspect the possible rhythmic patterns in sediment reorganization (erosion/deposition) induced by sediment transport and dune migration in response to the hydrodynamics. On a mobile seabed covered with various scales of defects (Fig. 2b to 2d), the rhythmicity of erosion and deposition zones indirectly matches the wavelengths of the various morphological defects that are generally grafted to dunes, independently from bedform migration rates (explanations illustrated in Fig.6).

The CWT has been carried out for the different time intervals (from  $I_1$  to  $I_4$ ) in two directions: (1) across the dune sections (alongshore), on the profiles A, B, C and D; and (2) along the dune sections (cross-shore) and parallel to the full dunes ( $DF_1$  to  $DF_6$ ).

The diagrams of CWT contain: (1) the contour diagram with space on the x-axis; (2) the frequency (spatial scale) or equivalent wavelength on the y-axis; and (3) the power or variance (which quantify the correlation between the signal and the wavelet basis) on the z-axis.

*Fig. 6. A conceptual representation of migrating bedform, between two times,  $T_1$  and  $T_2$ . a: simple case of a single bedform (BF) family. b: more complex case of a superimposed smaller bedform family (BF) over a dune family (DF) ( $x$  is or  $z$   $o_j$  the bedform in each family). In both the simple (a) and the more complex (b) cases, the morphological rhythmicities induced by altering erosion and deposition zones matches the wavelengths of the various families of migrating bedforms, whereas they are different from the pattern induced by the migration of the bedforms.*

## **2.5 2D dune migration**

Different methods for processing and evaluating the migration of dunes have been described in the literature as reviewed by Bartholomae et al. (2008). In the present research, a simple method to calculate the sand dune migration is implemented. This method aims to calculate the migration of dunes as a function of the local gradient of the bed elevation while the dune wavelength is maintained invariable in time.

The mathematical approach computes the migration rate  $\vec{V}_d$  in both dimensions X (parallel to the shoreline) and Y (orthogonal to the shoreline) for a given location  $(X_n, Y_n)$  as the following:

$$\vec{V}_d = \frac{\vec{M}}{\Delta t} = \left( \frac{\Delta Z}{\vec{M}} \right)^{-1} \cdot \frac{\Delta Z}{\Delta t} \quad (9)$$

where  $\vec{M}$  is the movement vector;  $\frac{\Delta Z}{\Delta t}$  and  $\frac{\Delta Z}{\Delta x}$  are the local gradient in time and space respectively.

In this study, the inverse of the local gradient  $\frac{\Delta Z}{\vec{M}}$  was expressed in the two dimensions of X

and Y as shown below:

$$\left( \frac{\Delta Z}{\vec{M}} \right)_n = \left( \left\{ \begin{array}{c} Z_{n+1} - Z_{n-1} \\ X_{n+1} - X_{n-1} \\ Z_{n+1} - Z_{n-1} \\ Y_{n+1} - Y_{n-1} \end{array} \right\}_i + \left\{ \begin{array}{c} Z_{n+1} - Z_{n-1} \\ X_{n+1} - X_{n-1} \\ Z_{n+1} - Z_{n-1} \\ Y_{n+1} - Y_{n-1} \end{array} \right\}_{i+1} \right) \cdot 1/2 \quad (10)$$

Equation 10 was applied for each dune section ( $X_n, Y_n$ ) between two successive surveys, at times  $t_i$  and  $t_{i+1}$ , which is illustrated in Figs 6a and 6c. Then, the local time gradient  $\frac{\Delta Z}{\Delta t}$  was calculated as:

$$\frac{\Delta Z_n}{\Delta t} = \frac{Z_{n,i} - Z_{n,i+1}}{t_{i+1} - t_i} \quad (11)$$

The components of dune movement ( $M_x, M_y$ ) have been calculated in both directions X and Y and the migration ( $\frac{\vec{M}}{\Delta t}$ ), calculated ( $V_x, V_y$ ), were investigated and correlated to the dune sediment transport ( $Q_{ld}, Q_{cd}$ ), derived from the local transport ( $q_{ld}, q_{cd}$ ) for the dune wavelength ( $\lambda_d$ ). The investigation was conducted during the period elapsed between two successive surveys  $\Delta t$  in both directions (Y, X) as described in Equations 12 and 13.

$$Q_{ld} = \iint_0^{\Delta t, \lambda_d} q_{ld} dx dt \quad (12)$$

$$Q_{cd} = \iint_0^{\Delta t, \lambda_d} q_{cd} dy dt \quad (13)$$

### 3 Results

### 3.1 Morphological variability of dunes

The form of the full dunes is complex with a series of morphological defects inducing different patterns in the mobility of the dune sections along each DF (DF<sub>1-6</sub>). This observation justifies our methodological approach focusing on the dune sections (D<sub>1</sub> to D<sub>24</sub>) distributed along the different dunes and along the profiles A, B, C, and D (Figs.2 and 3).

Fig.7.a and Fig.7.b present the variation of the dune angle ( $\gamma_d$ ), with respect to the y- axis, and the dune wavelength ( $\lambda_d$ ) for the 24 dune sections. The orientation, displayed by  $\gamma_d$ , underlines a non-homogenous distribution between dunes (from D<sub>1</sub> to D<sub>24</sub>). For each dune section, the orientation changes significantly in time between the different surveys (from S<sub>1</sub> to S<sub>5</sub>) as illustrated by the width of each boxplot (Fig.7a). Regarding  $\lambda_d$ , changes have been observed with an increasing trend from D<sub>1</sub> to D<sub>24</sub>. Such changes are trivial in time with an explained variance less than 10% for the different dune sections (width of each boxplot in Fig.7b). Hence, we can assume that their morphological changes do not affect their wavelength which is considered invariable for the different surveys (from S<sub>1</sub> to S<sub>5</sub>). Therefore, the main morphological changes of dunes are limited to their orientation (Fig.7a) and their elevation (Fig.3b).

The orientation of the dune sections is clockwise (negative values) and counter-clockwise (positive values) with respect to y-axis (Fig.2.a and Fig.6.a). The values of  $\gamma_d$  ranges between - 45° and + 45°. For the period of the current study, the mean values of  $\gamma_d$  are between - 15° and + 15°.

*Fig. 7 Boxplots showing the changes in the morphological characteristics of the dune sections (from D<sub>1</sub> to D<sub>24</sub>). Each boxplot represents the measurements collected during the different surveys (S<sub>1</sub>, S<sub>2</sub>, S<sub>3</sub>, S<sub>4</sub>, S<sub>5</sub>) for a given dune section: (a) the angle of the dune crestline with respect to y-axis  $\gamma_d$  (in this study, absolute values are considered), (b) the dune wavelength  $\lambda_d$ .*

Changes in the bed elevation, displayed by DoDs (Fig. 3b), show a series of positive and negative changes of the seabed elevation related to sediment accretion and erosion, respectively. In time intervals  $I_1$  and  $I_2$ , the whole dune field is mostly in erosion and mostly in accretion, respectively. Furthermore,  $I_3$  and  $I_4$  show both patterns of erosion and accretion. The most important variations are observed in time interval  $I_3$  with changes between -0.4 and +0.4 m, alternating from one dune to the other.

Overall, such changes exhibit a dune migration in the East-West direction (i.e. along the x-axis) since the dune morphology is recognizable between the different intervals, in particular the displacement of dunes during time intervals  $I_1$  and  $I_2$  and the variation in their sinuosity (Fig.3b).

The distribution of sediment patterns in  $I_3$  (and in a less extent in  $I_4$ ) highlights a minor pattern that reflects the migration of morphological defects oriented perpendicular to the main dunes, thereby reshaping the dunes and inducing a new organization of local sediment forms while maintaining the global forms of dunes. The sinuosity of dunes reveals low changes between  $I_2$  and  $I_3$  and seems to maintain its presentation, acquired during  $I_3$ , in  $I_4$ . During this last interval, the evolving morphological defects are also displayed (Fig.3).

### ***3.2 Dune dynamics in a wave-tide dominated environment***

During the study neap-spring cycle of 24 tides, the hydrodynamic conditions are controlled by the effects of waves and tides (Fig.4). The maximum wave height in the area under study reaches values higher than 2 m. The wave angle, calculated between the shoreline orientation (SW-NE) and the wave direction, varies mainly between  $0^\circ$  (for waves coming from WSW) and  $+45^\circ$  (for waves coming from WNW). The tidal flows are directed towards the East, strengthening the currents induced by waves in the E-NE direction. This interaction is mainly manifested during the flood stages. The sea bed tidal currents reach 0.65 m/s in  $T_{13}$  (spring

tides) and 0.08 m/s in  $T_3$  (neap tides) with a NW-NE direction, while the sea-surface tidal currents, oriented NW-N, vary between 0.15 m/s and 1.2 m/s at neap and spring tides, respectively. The mean direction, averaged during each tidal cycle, switches from NNW at spring tides to WNW at neap tides (Fig. 4).

The nearshore measurements of waves and currents highlight four energy episodes ( $E_1$ ,  $E_2$ ,  $E_3$  and  $E_4$ ; Fig. 4):  $E_1$  is the episode between  $T_1$  (27 Jan) and  $T_6$  (30 Jan) showing neap tides and moderate waves with an average height lower than 1 m and coming from W;  $E_2$  is the episode between  $T_7$  (30 Jan) and  $T_{13}$  (3 Feb) with spring tides and W-SW waves of 1.5-2 m height;  $E_3$  is the episode between  $T_{14}$  (3 Feb) and  $T_{19}$  (5 Feb) with spring tide and high to moderate waves of SW direction and 1.5 m height;  $E_4$  is the episode between  $T_{20}$  (5 Feb) and  $T_{24}$  (7 Feb) with neap tides and low wave energy, coming from SW and lower than 1 m of height.

The energy episodes  $E_1$ ,  $E_2$ ,  $E_3$  and  $E_4$  are related respectively to the morphology of dunes during the intervals  $I_1$  (between  $S_2$  and  $S_1$ ),  $I_2$  (between  $S_3$  and  $S_2$ ),  $I_3$  (between  $S_4$  and  $S_5$ ) and  $I_4$  (between  $S_6$  and  $S_5$ ).

During the first episode  $E_1$ , the current velocities are limited to 0.5 m/s and 1 m/s at 1 m above the sea-bed and the sea-surface, respectively. The wave-tide angles  $\alpha_b$  and  $\alpha_s$  are of  $45^\circ$  and  $60^\circ$ , respectively. Clockwise and counter-clockwise wave angles are observed with a mean  $|\theta|$  around  $65^\circ$  or  $10^\circ$  (values seem to be not around  $45^\circ$ ). The dune angles take relatively small values and seem to be close to zero when they are orthogonal to the shoreline ( $|\gamma_d|$  less than  $20^\circ$ ). This hydrodynamic scenario of low incidence and small waves generate moderate components of longshore (orthogonal to dunes) and cross-shore (parallel to dunes) transport responsible for a limited mobility of sediments. The morphological gradient remains approximately zero with gradual changes in bed elevations induced by the current velocities (Fig. 3.b).

During the second energy episode  $E_2$ , the current velocities increase to reach a maximum of 1 m/s and 1.8 m/s respectively at 1 m above the sea-bed and the sea-surface while the wave-tide angles ( $\alpha_b$  and  $\alpha_s$ ) don't exceed  $45^\circ$ . Waves with increasing height and significant obliquity ( $|\theta|$  around  $45^\circ$ ) enhance the induced currents responsible for the longshore transport. The cross-shore component is also important in this episode since the wave height reaches its maximum of 2 m. Such conditions (strong tidal currents and wave activity) are responsible for a significant transport of sediment across the dune sections and some changes in their orientation (as illustrated in Fig.3.b) with an angle  $\gamma_b$  between  $35^\circ$  and  $45^\circ$  leading to a high sinuosity.

This large sediment supply is clearly observed for the interval  $I_2$  (Fig.3b), with a positive bed elevation (maximum values reaching 0.4 m height) along the whole dune field showing different patterns of sediment accretion.

The tidal currents maintain their velocities, observed in  $E_2$ , at the beginning of  $E_3$  (during  $T_{14}$  and  $T_{17}$ ) and decrease significantly at the end of the episode ( $<1.5$  m/s and 0.5 m/s for sea-surface and 1 m above sea-bed currents, respectively). Regarding the wave activity, it decreases slightly (compared to  $E_2$ ) with smaller heights ( $H_1 = 1.8$  m) and low obliquity (i.e. waves coming from SW with  $|\theta|$  around  $55^\circ$ ) generating a moderate longshore (cross-dune) transport. Such energy conditions allow the sediment gained during the previous episode to be redistributed within the dune field; they are responsible for a new organization of dunes and evolving morphological defects.

During the last energy episode  $E_4$ , the velocity of tidal currents decreases significantly with a mean wave-tide angle of  $30^\circ$ . The low wave activity at neap tide conditions limits the morphological changes and decreases the changes in the organization of the dunes. This episode is largely favorable for maintaining the new morphological organization, presented in  $E_3$ , and developing superimposed bedforms whose build-up should have started at the end of the  $E_3$  when the energy conditions were decreasing.

Finally, the key role of waves in this environment has been analyzed separately from the tidal effects in Fig.8 where the two components of the energy flux (i.e cross-dunes  $EF_{cd}$  and long-dunes  $EF_{ld}$ ) have been calculated for each dune section during the different energy episodes  $E_1$  (tides  $T_1 - T_6$ ),  $E_2$  (tides  $T_7- T_{13}$ ),  $E_3$  (tides  $T_{14}-T_{19}$ ), and  $E_4$  (tides  $T_{20} - T_{24}$ ). Both components account not only for the wave characteristics (the amount of energy related to the waves and their direction) but also for the dune orientation. The evolution of  $EF_{cd}$  and  $EF_{ld}$  shows a large variability during the energy episodes  $E_2$  and  $E_3$  when the fluxes become higher than 2000 J/m.s and 1000 J/m.s respectively (Fig.8). Within each episode, the components of the energy fluxes highlight a series of changes which are not necessarily uniform in time, nor for all the dune sections. High spatial oscillations of the energy fluxes have been observed with a frequency of 6 dune sections approximately showing single responses for each dune section as a function of its orientation (angle  $\gamma_b$ ; Fig. 7a). Positive and negative components are produced for clockwise and counter-clockwise dune angle ( $\gamma_b$ ) respectively.

*Fig.8 The components of the energy flux across ( $EF_{cd}$ ) and along ( $EF_{ld}$ ) the dunes for the different energy episodes ( $E_1$  to  $E_4$ ), dune sections ( $D_1$  to  $D_{24}$ ) and tides ( $T_1$  to  $T_{24}$ ). x-axis: the dune section ( $Dx$ ); y-axis: the tide ( $Tx$ ); z-axis: the oriented energy flux illustrated by the color scale (positive values towards East, negative values towards West) .*

### **3.3 Morphological evolution of dune defects at different ranges of scales**

The stochastic approach of CWT has been applied to analyze the complex morphological pattern of dunes and their changes (Fig. 2) to identify the multiscale morphological modulations of dunes in response to the hydrodynamics.

The DoDs measurements (Fig.3b) have been used to investigate the modulations of the dune changes due to sediment transport and resulting dune migration during the different time-intervals: (1) perpendicular to dunes along the profiles A ( $D_1$  to  $D_6$ ), B ( $D_7$  to  $D_{12}$ ), C ( $D_{13}$  to  $D_{18}$ ) and D ( $D_{19}$  to  $D_{24}$ ) (Fig. 9); and (2) parallel to dunes, along a series of four profiles

perpendicular to A, B, C and D. As explained in section 2.4, the CWT analysis allows to extract

rhythmic patterns in the dune changes (erosion/deposition zones) that indirectly matches the wavelengths of the various morphological defects. We use it to describe the presence of morphological defects and their evolution.

First, the morphological modulations of dune sections (from  $D_1$  to  $D_{24}$ ) have been investigated as displayed by the diagrams of Fig.9, in the cross-dune (alongshore) direction. The distribution of the CWT spectrum is non-uniform with altering bands of high and low power. The well-structured bands with high power correspond to the spatial frequencies of  $\sim 12.8$  m,  $\sim 6.4$  m and  $\sim 3.2$  m. They highlight the existence of several modulations of morphological changes structured in space (depending on the profiles) and time (depending on the time-intervals). The modulation of  $\sim 12.8$  m is well-identified in the CWT diagrams; it represents the mean wavelength of dunes in the *Baie de Somme* (see section 2).

The small modulations of  $\sim 3.2$  m display non-homogenous patterns with different spatial frequencies. They also vary from the onshore (profile D) to the offshore (profile A) positions. The modulations of  $\sim 6.4$  m are arranged according to a series of irregularities disconnected between them and organized parallel to the dune crestlines (perpendicular to x-axis).

The morphological modulations of  $\sim 3.2$  m and  $\sim 6.4$  m are observed in  $I_1$  with non-organized forms separately displayed according to the scale range. The majority of these modulations disappear in  $I_2$  for the different profiles while they emerge in  $I_3$  with well-structured forms clearly delineated for the profile D. They are homogeneously represented for the last interval with a morphological connection between the small ( $\sim 3.2$  m) and the large ( $\sim 6.4$  m) modulations, particularly observed for the onshore dunes (Profiles C and D). These morphological forms (i.e.  $\sim 3.2$  m and  $\sim 6.4$  m) should be associated to the dune defects (observed in Fig.2.b, 2.c and Fig.3b). They correspond to superimposed bedforms, and are

classified as small and medium dunes (Ashley, 1990), respectively. Indeed, the small and medium superimposed dunes have been partly identified during  $I_1$  as a series of irregularities (blue spots displayed in Fig.3b). Their destruction has eventually occurred during  $I_2$  and at the beginning of  $I_3$  while their significant proliferation was produced at the end of  $I_3$  and during  $I_4$  (pink spots displayed in Fig.3b), in particular for onshore dunes (from  $D_{18}$  to  $D_{24}$ ).

Therefore, the superimposed dunes seem to be more pronounced in  $I_1$  and  $I_4$ , in particular for the onshore dunes (lines D and C in Fig. 9), under moderate wave conditions and neap tides. Their density is reduced at the beginning of  $I_3$  and during  $I_2$  when their development is limited.

*Fig.9 CWT diagrams of dune morphological changes in the cross-dune (alongshore) direction along the four profiles A, B, C, and D (see Fig. 2.a), during time intervals  $I_1$  to  $I_4$ , between the different topographic surveys S1 to S5. The multi-space-scale features (y-axis of the CWT diagram) identified are:  $\sim 12.8$  m,  $\sim 6.4$  m and  $\sim 3.2$  m. x-axis: the distance; y-axis: the frequency (spatial scale) or equivalent wavelength; color scale: the power or variance (which quantify the correlation between the signal and the wavelet basis), from red-yellow (low) to blue-pink (high).*

Second, the morphological variability of the dunes has been investigated for each full dune ( $DF_1$  to  $DF_6$ ) between the successive surveys to identify the defects of dunes along their crestlines, in the cross-shore direction (Fig. 10).

Here, the main modulations are described by the scale ranges of  $\sim 25$  m. They vary in distribution and density as a function of DF (from  $DF_1$  to  $DF_6$ ) and the time-intervals. They are particularly identified from the second interval  $I_2$  for  $DF_1$  to  $DF_4$ , and conserved in  $I_3$  and  $I_4$  for the different full dunes (Fig.10).

Similar defects with a mean wavelength of  $\sim 24$  m, observed in the dune field (Fig.2b), are associated to the sinuosity of dunes along their crestlines. Changes in the dune crestline sinuosity have been observed in  $I_2$  in response to the energetic episode  $E_2$  with high wave

obliquity. The evolving sinuosity is maintained for the rest of time under moderate hydrodynamic conditions at the end of  $E_3$  and during  $E_4$ .

Furthermore, small modulations around  $\sim 1.6$  m and orthogonal to dunes have been observed in the CWT (Fig.10). They are visible along the dune field (Fig.2.b) and correspond to superimposed small dunes probably formed at the end of the ebb phase when the dune field is drained. These features are remodeled quickly, but are visible on the DEMs, especially on 6<sup>th</sup> and 9<sup>th</sup> February 2014 (Fig. 3a), and on the DoDs of intervals I3 and I4 (Fig. 3b).

In summary, the spectral analysis has proven that the spatial distribution of the morphological defects and their densities vary at different ranges of length scales (frequencies) across (Fig. 9) and along the dunes (Fig.10). This exhibits that dunes change with various multiscale patterns due to the migration and the morphological changes of superimposed bedforms and defects that can be presented into 3 groups: (1) superimposed medium and small dunes of  $\sim 6.4$  m and  $\sim 3.2$  m respectively, mostly parallel to the dune crestline orientation; (2) superimposed small dunes of  $\sim 1.6$  m, mostly orthogonal to dune crestline orientation; (4) dune sinuosity.

*Fig.10: CWT diagrams of the dune morphological changes along the dunes DF1 to DF6 (Fig. 2a) (crossshore direction) during time intervals I1 to I4, between the different topographic surveys S1 to S5. The multi-space-scale features (y-axis of the CWT diagram) identified are:  $\sim 25.6$  m,  $\sim 12.8$  m,  $\sim 6.4$  m and  $\sim 3.2$  m. x-axis: the distance; y-axis: the frequency (spatial scale) or equivalent wavelength; color scale: the power or variance (which quantify the correlation between the signal and the wavelet basis) from red-yellow (low) to blue-pink (high).*

### ***3.4 Dune migration vs estimated sediment transport components***

The components of migration  $V_x$  and  $V_y$  have been computed to identify the mobility of dunes (Fig.11). The components  $V_x$  (grey circles; Fig. 11) and  $V_y$  (black circles; Fig.11) correspond

to the dune migration across and along the dunes, respectively. They vary in space (from  $D_1$  to  $D_{24}$ ) and time (from  $I_1$  to  $I_4$ ). This variation is a function of the dune orientation (angle  $\gamma_b$ ) and the nearshore hydrodynamic conditions of waves, tides and currents.

$V_y$  reveals a series of changes in the migration of the dune sections along a same full dune (for example  $D_1, D_7, D_{13}, D_{19}$  of  $DF_1$ ); such changes are differently manifested for the time intervals. It takes mostly positive (onshore direction) values and reaches its maximum (+ 0.25 m/day) during the energy episodes  $E_2$  and  $E_3$ .

Moreover, the cross-dune migration  $V_x$  oscillates between positive (until + 0.45 m/day) and negative (until - 0.45 m/day) changes corresponding to the clockwise and counter-clockwise changes of dunes, respectively. Such changes are relatively limited during  $E_1$  and  $E_4$  where wave activity decreases at neap tides.

In the light of results provided by Fig.11 the components  $V_x$  and  $V_y$  exhibit some differences in the dune migration between onshore ( $D_{13}$  to  $D_{24}$ ) and offshore ( $D_1$  to  $D_{12}$ ) dune sections. since the effects of hydrodynamic forces are relatively higher in areas further away from the shoreline. Both components reveal significant changes for the offshore dunes (i.e.  $D_1$  to  $D_{12}$ ) with values varying between +/- 0.18 m/day ( $E_1$  and  $E_4$ ) and +/- 0.4 m/day ( $E_2$  and  $E_3$ ). These results underline the higher effects of hydrodynamic forces (tides, waves) in areas further away from the shoreline.

Generally, the migration along the dunes  $V_x$  has proven to be significantly important during high energy episodes (spring tides with high wave obliquity at  $E_2$  and the beginning of  $E_3$ ) with a mean explained variance > 60% of the total migration. This percentage is differently manifested for moderate hydrodynamic conditions with ~ 32% (neap tides with low wave obliquity at  $E_1$ , the end of  $E_3$  and  $E_4$ ). During these conditions, ~32% of the migration is

produced along the dunes ( $V_y$ ).  $V_y$  takes mainly positive values which underlines the dominance of the onshore dune migration during the period of study.

*Fig.11. Dune Migration: cross-dune migration  $V_x$  (grey circles) and long-dune migration  $V_y$  (black circles) for the dune sections D1 to D24.*

The relation between the dune migration and the sediment transport quantities in the cross- and long-dune directions has been explored. These quantities, respectively  $Q_{cd}$  and  $Q_{ld}$ , vary in time and space as a function of the characteristics of the dunes (i.e. wavelength, and angle) and external forcing (i.e. wave-tide conditions). The correlations between  $Q_{cd}$  ( $Q_{ld}$ ) and  $V_x$  ( $V_y$ ) has been simulated and illustrated respectively in Figs.12 and 13. The goodness of the fit between both physical quantities is clearly observed with mean coefficients  $R^2$  higher than 70%. They are higher for offshore dunes ( $D_1$  to  $D_{12}$ ), ranging between 78% and 88%, and decrease for the onshore dunes ( $D_{13}$  to  $D_{24}$ ) where the morphological changes are probably controlled by additional external mechanisms (e.g. the effect of wind to move the dry particles of sediments). Best correlations have been identified between  $V_y$  and  $Q_{ld}$  ( $R^2 > 0.8$ ) while they decrease slightly for the cross-dune migration  $V_x$  with  $Q_{cd}$  ( $R^2 = 0.7 - 0.8$ ).

The highest  $R^2$  values are recorded for  $E_2$  and  $E_3$  (0.75 - 0.8 for the cross-dune direction, 0.81-0.88 for the long-dune direction) and the lowest for the time  $E_1$  and  $E_4$  (0.7-0.8 and 0.75-0.78, respectively), which correspond respectively to the periods of increasing (high wave activity and spring tides) and decreasing (moderate wave activity and neap tides) hydrodynamic conditions.

Overall, the mobility along the dunes ( $V_y$ ) responds faster than that across the dunes ( $V_x$ ) to the changes in the sediment transport components in the onshore-offshore direction.

This difference could be explained probably by a shorter time-lag between the correlated  $V_y$  and  $Q_{ld}$  with a mean order of 3 tidal cycles while the mean time-lag between the correlated  $V_x$  and  $Q_{cd}$  is about 5 tidal cycles.

*Fig.12 The component  $V_x$  of the dune migration (grey circles) vs the cross-dune sediment transport  $Q_{cd}$  (grey crosses) for each of the dunes (DF1 to DF6) and dune sections (D1 to D24) and for the time intervals 1 to 4.  $R^2$  coefficients are also illustrated.*

*Fig.13 The component  $V_y$  of the dune migration (black circles) vs the long-dune sediment transport  $Q_{ld}$  (black crosses) for each of the dunes (DF1 to DF6) and dune sections (D1 to D24) and for the time intervals 1 to 4.  $R^2$  coefficients are also illustrated.*

#### 4. Discussion

In this section, the main findings of this work are synthesized and summarized in Figure 14 and Table 1. The dynamics of dunes in the Baie de Somme and their morphological changes are explained in relation with high and low energy episodes of various tide and wave conditions.

*Fig.14 Conceptual synthesis summarizing the results related to the dune dynamics in the Baie de Somme for high- and low-energy episodes.*

*Table 1. Comparison of the dune dynamics between high and low energy episodes.*

The intertidal dunes of the Baie de Somme studied in this paper vary in orientation and morphological characteristics (e.g. changes in sinuosity, development or attenuation of the superimposed bedforms). This work is conducted under mixed wave-tide conditions during a

full neap-spring cycle of 24 tides (27 January – 09 February 2014) with moderate to high wave activity (maximum height of 2 m).

Here, we investigate the dynamics of dunes by the use of two simplifications: (1) the six large dunes ( $DF_1 - DF_6$ ) have been divided into 24 independent dune sections (D1 to D24) in order to analyze the complex evolution of dunes as a response of wave-tide conditions (Fig.2 and Fig.3); (2) the wavelength of the dune sections during a full neap-spring tidal cycle does not show any significant changes in time (Fig. 3); that's why it has been considered constant during the study period. Similar assumptions have also been documented in other works (e.g. Allen, 1968; 1973; 1976; Hendershot et al., 2018) where dunes conserve their length over the course of the tidal cycle.

Contrary to the wavelength ( $\lambda_d$ ), the elevation and the orientation of the dune sections respond rapidly to the fluctuating hydrodynamic conditions. The variation of the dune geometry is associated with clockwise/counter-clockwise changes in the orientation angle and positive/negative changes in the elevation of dunes, respectively. Such variation of geometry involves the dune migration which is mainly produced towards NE in Baie de Somme following its polarity (Michel et al., 2017).

The interaction between the tide-wave driven forces and the dune morphology and migration has been investigated in Baie de Somme by considering: (1) the bedload and the suspended sediment transport calculated from the current velocities measured 1 m above the bottom and the sea surface, respectively; (2) the effect of tide-wave interaction through the use of the wave angle, calculated with respect to tidal currents.

On the basis of the characteristics of the 1-minute hydrodynamic measurements, the study period has been divided into four energy episodes ( $E_1$  to  $E_4$ ) which have been related to four-time intervals ( $I_1$  to  $I_4$ ) of dune changes. Only the final morphological evolution of dunes as a

response to the previous wave-tide driven forces has been measured and used to understand the dynamics of the intertidal dunes.

#### **4.1. Morphological evolution of intertidal dunes as a response to tide-wave conditions**

Some physical processes may explain the relationships between the different morphological observations and the hydrodynamics measurements during the study neap-spring tidal cycle. They can be drawn from our analysis.

At the scale of the semi-diurnal tidal cycle, the variations in sediment transport lead to some morphological remodeling of the dune bedforms. Indeed, when the water level falls during the ebb stages, waves increase in height with an obliquity of around  $\pm 45^\circ$ . The sediments move mainly as bedload and accumulates/erodes along the slope eventually inducing changes in the dune geometry (i.e. elevation and/or orientation). In this case, negative/positive wave obliquity leads to eroding/accreting patterns. Conversely, when the water level rises during the flood stages, the concentration of the suspended sediment at the sea-surface increases. At this stage, sediments are transferred from the crest to the trough of the dunes thereby decreasing the dune slope steepness.

During the study period, several hydrodynamic conditions have induced different morphological responses of dunes from modest to complex ones. For current velocities varying between 0.5 m/s and 1 m/s and moderate wave activity ( $E_1$  and  $E_4$ ), the dunes in Baie de Somme have a low activity; they are well-structured forms with a strong pattern of superimposed bedforms and a moderate sinuosity. These forms change to complex ones with a series of morphological discontinuities when the current velocities increase reaching values of 1.8 m/s during  $E_2$  and  $E_3$  energy episodes. Similar suggestions have been outlined by Ashley (1990), Terwindt and Brouwer (1986); Larcombe and Jago, (1996) works where the

morphological discontinuities of dunes have been revealed when the current velocity exceeds 0.7 m/s.

Here, the hydrodynamic conditions of high wave obliquity and tidal currents contribute in the evolving the crestline sinuosity along the dunes and the induced morphological defects that take place after the beginning  $I_3$  when the energy activity decays. The high energy episodes of spring tides in the Baie de Somme are responsible for developing the morphological dune discontinuities and boosting a potential physical mechanism of bifurcation (not clearly observed from observations during the study period).

In the light of the results, provided by the bed elevation changes (Fig.3b), dune geometry (Fig.7) and the hydrodynamics (Fig.4), a series of physical mechanisms can be presented to explain the dynamics of dunes during the period of study. The dune field does not exhibit any significant changes during periods of moderate activity of waves and currents (e.g.  $I_1$ ). Then, the high energy conditions of  $E_2$  and the beginning of  $E_3$  contribute in an increasing sinuosity of dunes and an important sediment supply inducing dune morphological development and migration. This supply is distributed within the dune field at the end of  $I_3$ ; which is responsible for a new organization of dunes and evolving morphological defects. Finally,  $I_4$  is largely favorable for maintaining the new morphological organization, presented in  $I_3$ , with decreasing hydrodynamic conditions. This context is encouraging for the development of superimposed bedforms.

Accordingly, the changes in the nearshore wave-tide conditions are responsible for the variability of the dune sections during the different time intervals and exhibit a strong redistribution of sand, responsible for the morphological variability of the dunes and their organization. These changes are produced mainly following two mechanisms: (1) the development of superimposed small to medium dunes over the large dune sections observed under low energy conditions of wave and tides (e.g. observed during the episodes  $E_1$ , at the end of  $E_3$  and  $E_4$ ); (2) the sinuosity of dunes induced by variable changes in their crestline orientation as a response to a significant sediment

mobility across the dunes produced at spring tides and high wave energy conditions (e.g. observed during  $E_2$ ).

## 4.2 Development of the dune defects in relation with the energy episodes

A range of defects with multiple sizes and shapes has been observed above the dunes of the Baie de Somme exhibiting the dynamics of the dune field in relation with the interaction between their morphological characteristics and the wave-tide activity (Fig.14).

The morphological defects identified across and along the dunes stress their spatial multiscale variability between each of the time intervals: (1) the crestline sinuosity (with wavelength of  $\sim 25.6$  m) along the full dunes, (2) large and small superimposed bedforms, arranged parallel to the dune crestlines with  $\sim 6.4$  m and  $\sim 3.2$  m wavelength. These defects have been differently manifested in time according to the combined effects of wave and tides associated to each energy episode.

The smallest morphological defects, with  $\sim 1.6$  m wavelength, have been observed perpendicular to the dune crestlines for the different energy episodes; they are mainly related to the tidal currents during the ebb and the flood phases.

The development and destruction of the morphological defects, observed during the study period in response to various hydrodynamic conditions, should be explained by a series of physical mechanisms that are presented here as hypotheses with the aim to elucidate the relationship between the different forms of defects.

Under moderate wave-tide activity (i.e. neap tides and moderate waves;  $E_1$  and  $E_4$  periods), the small superimposed bedforms ( $\sim 3.2$  m), generally grafted to dunes, grows when dunes exhibit little changes; which is the case for  $I_1$  (Fig.3.b), the end of  $I_3$  and  $I_4$  (Fig.3.b). They maintain their organization as long as the hydrodynamic driving forces are limited. Their growth and their increasing density expand their length scales (Figs. 9 and 10). The development of the small superimposed bedforms should be rapid, with a timescale of

approximately 3 days (i.e. time spacing between the first and the second survey) to act probably as nucleation points for the development of the new larger superimposed bedforms with higher length scales (~6.4 - 3.2 m). They are created at the final stage of the defect growth during the intervals 1 and 4.

Then, the multi-scale superimposed bedforms of the dunes should be strongly connected since the growth of the small bedforms leads to the development of the large ones due to a progressive build-up taken place during the period of moderate wave-tide activity. The low density of the small defects can behave as inhibitors of the dune bedforms. These morphological changes are established when the dunes show a progressive build-up of some pronounced defects under moderate hydrodynamic conditions (i.e. the dune field displays limited changes of accretion/erosion above the dune surface; Figs. 3.b, 8 and 9).

During the high-energy episodes (i.e. spring tide strong waves;  $E_2$  and the beginning of  $E_3$ ), the morphological system is unstable because the wave-tide driven forces perturb the bedforms above the dunes and provoke their destruction. These hydrodynamic conditions exhibit changes in the orientation of the dune crestlines, under a significant wave obliquity, and a high activity of transport for supplying the dune field and inducing a new redistribution of sediments. When the sediment flux increases, the resultant fast morphological changes promote the self-organization of the dunes.

Under these hydrodynamic conditions, not favorable to the dune stability, evolving morphological irregularities should take place to be built-up at the end of  $I_3$  when the energy activity increases. These conditions could be also favorable for boosting a new physical mechanism of bifurcation (e.g., Colombini and Stocchino, 2008; Ewing et al., 2006; Huntley et al., 2008; Werner and Kocurek, 1999).

The presence of the superimposed bedforms is reduced during high fluxes responsible for their possible vanishing. The concept of bedform vanishing has been studied in the Parteli et

al. (2014) works where a short review on the physics of dune formation has been presented. From experiments, they have demonstrated that an isolated sand bar breaks into a chain of barchans under unidirectional water stream. Under this condition, the local shear stress is set to zero thereby fully neglecting the sediment flux.

In the same context, several works have investigated the dynamics of the bedforms which is mainly controlled by complex interactions between flow, sediment transport and evolving morphology (e.g. Coco and Murray, 2007). Indeed, the bedforms are developed by wave and current-induced flows (Flemming, 1980) under intermediate flow conditions, between the thresholds for grain movement and sheet flow (Dalrymple and Rhodes, 1995). When the flow intensity exceeds the critical condition of sediment movement, the sea-bed is changing and becoming unstable inducing the birth of morphological irregularities. Such morphological irregularities reach a maximum in their height and length when shear stress increases. Under the conditions of sheet flow criterion, bedforms are washed-out and upper-plane bed sheet flow occurs (Southard and Boguchwal, 1990; Soulsby and Whitehouse, 2005; Camenen, 2009).

When the shear stress decreases below the threshold of initiation of sediment motion, the morphological irregularities can continue lying on the seabed inactive during low flow conditions (Soulsby et al., 2012). The wash-out or sheet flow phases can involve a bedload sediment transport responsible for the migration of the bedforms (Traykovski et al., 1999; Camenen and Larson, 2006; van Rijn, 2007).

Thereby, the wash-out (progressive vanishing) and sheet flow conditions of the morphological bedforms is strongly related to their morphology (e.g. orientation and localization, shear stress, sediment motion) and to the tide-wave driven forces (e.g. including their amplitude and their velocity).

The density of the superimposed bedforms plays a key role in controlling the evolution of the dunes under the nearshore hydrodynamic conditions. Indeed, dunes with low density of the superimposed bedforms resist more to the morphological changes (i.e. height and length). On the other hand, dunes with higher density experience larger changes. Similar findings, suggesting the major role of the superimposed bedforms in controlling the overall morphology of the dunes, have been underlined in the works of Werner and Kocurek (1997). They argue that, based on the numerical modelling of aeolian sand dynamics, higher densities of superimposed bedforms result in faster field-scale reorientation rates compared to more linear dunes with a lower proportion of superimposed bedforms.

Accordingly, the high density of the superimposed bedforms is inversely related to the sediment fluxes along the dunes. When the sediment flux becomes low, the resultant slow morphological changes promotes the development of dunes and the growth of the superimposed bedforms. On the other hand, when this sediment transport flux becomes more significant, the dunes grow faster with lower density of the superimposed bedforms. The evolution of these forms should influence the crestline orientation changes of the dunes and, finally, their splitting (Huntley et al., 2008).

### **4.3 Cross- and long-tune migration vs tide-wave conditions**

Averaged over the entire observation period, dunes have shown a varying asymmetric shape with a polarity changing from NE to SW according to the hydrodynamic conditions (Michel et al., 2017). Contrary to the previous studies (e.g. Knaapen, 2005) showing that the dune migration follows the direction of their steepest slope, the movement of the dunes in Baie de Somme changes during the neap-spring tidal cycle exhibiting a series of clockwise and counter-clockwise shifts in response to tide-wave dynamics.

By the use of a simple conceptual model, the total dune movement has been decomposed into two geometrical components, across and along the dunes, and correlated to the physical mechanisms of sediment transport. The approach used here is based on a series of assumptions: (1) a weak dependence between the cross- and long-dune migration for their correlation with the sediment transport across and along the dunes; (2) a linear relationship between the dune migration and the sediment transport; (3) the alongshore wave height gradients is neglected for the calculation of the longshore sediment transport; (4) the dune roughness is not considered for studying the connection between the hydrodynamics forcing and the morphological defects.

Results have shown that more than 65% of the dune migration occurs in the cross-dune direction during the high energy episodes (i.e. spring tides and significant waves) while it is limited to 32% for the moderate energy episodes (Fig.14, Table 1). The long-dune migration has been correlated to the cross-shore sediment transport (equivalent to the long-dune transport when  $\gamma_b = 0$ ) while the cross-dune migration has been associated with the long-shore transport (equivalent to the cross-dune transport when  $\gamma_b = 0$ ). Correlations are strongly significant with mean coefficients  $k^2$  ( $p < 0.05$ ) higher than 70%. The relationship between the migration of the dunes and the sediment transport are controlled by the characteristics of the dunes (i.e. wavelength, and orientation) and the external forcing (i.e. wave-tide conditions).

At short timescales, the correlations are more satisfactory along the dune crestline (where the morphological changes are faster). Furthermore, the migration of dunes along their crestlines is related to the onshore-offshore sediment transport rather than the cross-dune transport (which is mainly controlled by the wave obliquity).

For some dunes, the physical match between their migration (i.e.  $V_y$  and  $V_x$ ), and the sediment transport quantities ( $Q_{ld}$  and  $Q_{cd}$ ) is not significant enough which is caused potentially by the significant dependence between both cross-and long-movement of dunes. Thereby, the

simplified approach used to determine the components of the dune migration is limited to the cases where the physical dependence between both components is weaker.

Accordingly, the external forcing and the characteristics of the dunes have a strong influence on controlling the dune movement. Dunes which move perpendicular (parallel) to their form change slower (faster) as a response to the along-dune (cross-dune) sediment transport. Similar hypotheses have been also outlined by the works of Turki et al. (2013) where the variability of the shoreline has been studied according to its morphological characteristics and the changing nearshore hydrodynamics. They have demonstrated that the response of the beach to the energy is such that the greater the length of the beach and its sediment grain size, the slower the response; additionally, the higher the energy is, the faster the response becomes.

## Conclusion

In mixed tide-wave environments, the dynamics of the intertidal dunes reveals a series of complex mechanisms related to the development of several defects (i.e. superimposed bedforms and crestline sinuosity) with different ranges of scales. The development of the superimposed small and medium dunes is induced by a progressive build-up of dunes in case of low energy conditions (neap tides, low wave activity) while changes in the sinuosity of the dune crestlines can be responsible for a potential self-organization along the dunes in case of high energy conditions (i.e. spring tides, moderate wave energy).

Using the assumption that the dune wavelength does not change in time, the migration of the dunes along and across their forms (respectively in the cross- and long-shore directions) have been quantified from a simple conceptual model, proposed in this research, and correlated with the cross- and long dune sediment transport components. More than 60% of the dune mobility is produced across their crestlines in response to high tide-wave conditions; it is

limited to 30% where the energy activity decreases. The cross-dune migration is strongly correlated to the long-shore sediment transport while the migration of dunes along their forms is matched to cross-shore transport with  $R^2$  higher than 0.7. The correlation coefficients increase to a mean value of 0.83 for high energy episodes. The key role the wave obliquity plays in the migration of dunes and their crestline changes has been demonstrated during high wave-tide conditions. The dune migration should also be controlled by the dune size sediment properties and the roughness of the bed, for which an accurate description and quantification is needed.

Overall, our finding indicates that the multiscale variability of bedforms and their mobility are strongly related to the physical mechanisms involved in the hydrodynamic-driven sediment transport. These natural systems are constantly in motion and tend to be non-conservative under changing hydrodynamic conditions and morphological characteristics. Combining different stochastic, physical and numerical approaches is greatly required to gain insight in the dynamics of bedforms from short timescales in linkage with the extreme events to large timescales related to climate change context.

## Acknowledgments

This work was supported by a grant from DGA (Direction Generale de l'Armement) and Région Haute-Normandie, and by financial findings from INSU-CNRS (project EC2CO FORSOM). Authors want to thank Adrien Cartier (GéoDUNES) for its assistance during the hydrodynamic measurements and Michel Simon for his help on the field. Finally, the authors would like to express their gratitude to the editor and the unknown reviewers for the excellent suggestions, which improved the original manuscript.

## References

Allen, J.R.L., 1968. The nature and origin of bedform hierarchies. *Sedimentology* 10, 161–172.

Allen, J.R.L., 1973. Features of cross-stratification due to random and other changes in bed forms. *Sedimentology*, 20, 189-202.

Allen, J.R.L., 1976. Computational models for dune time-lag: general ideas, difficulties, and early results. *Sed. Geol.*, 15, 1–53.

Bailard, J.A., 1981. An energetics total load sediment transport model for a plane sloping beach. *J. Geophys. Res.* 86, 10938–10954.

Bailard, J.A., Inman, D.L., 1981. An energetics bed load model for a plane sloping beach. *J. Geophys. Res.* 86, 2035–2043.

Bartholdy, J., Flemming, B.W., Bartholomä, A., Ernstsens, V.B., 2005. Flow and grain size control of depth-dependent simple subaqueous dunes. *J. Geophys. Res. Earth Surf.* 110, F04S16.

Bartholdy, J., Ernstsens, V.B., Flemming, B.W., Winter, C., Bartholomä, A., 2008. On the development of a bedform migration model. MARID- Leeds, United Kingdom

Bellessort, B., Migniot, C., 1986. Catalogue of sediment deposition along the French coasts: coasts of the North Sea and the English Channel. Part C, From the Seine Bay to the Mont Saint Michel. /*Colloq. Dir. des Etudes Rech. Electr. Fr.*, \*61\*, 231–406.

Bellessort, B., Migniot, C., 1987. Catalogue sédimentologique des côtes françaises. Côtes de la Mer du Nord et de la Manche: de la Baie de Somme à la Baie de Seine. Eyrolles, 135–230.

Bennett, S.J., Best, J., 1995. Mean flow and turbulent structure over fixed, two-dimensional dunes: Implications for sediment transport and bedform stability. *Sedimentology* 42, 491-513.

Best, J., Kostaschuk, R.A., 2002. An experimental study of low-angle dunes. *J. Geophys. Res. Oceans* 107 (C9), 3135-3154.

Bartholomä, A., Schrottke, K., Winter, C., 2008. Sand wave dynamics: Surfing between assumptions and facts. In: Parsons, D., T. Garlan and J. Best (eds) *Marine and River Dune Dynamics*, p. 17-24.

Boyd, R., Dalrymple, R. W., Zaitlin, B. A., 1992. Classification of clastic coastal depositional environments. *Sediment. Geol.*, 80(3-4), 122-150. doi:10.1016/0037-0738(92)90037-R.

Camenen, B., Larson, M., 2006. Phase-lag effects in sheet flow transport. *Coast. Eng.* 53, 531-542. doi:10.1016/j.coastaleng.2005.12.003.

Camenen, B., 2009. Estimation of the wave-related ripple characteristics and induced bed shear stress. *Estuar. Coastal Shelf Sci.* 84, 553-564. doi:10.1016/j.ecss.2009.07.022.

Charru, F., Andreotti, B. and Claudin, P., 2013. Sand ripples and dunes. *Ann. Rev. Fluid Mechanics*, 45, 469-493.

Cheng, H.Q., Kostaschuk, R., Shi, Z., 2004. Tidal currents, bed sediments, and bedforms at the South Branch and the South Channel of the Changjiang (Yangtze) estuary: implications for the ripple-dune transition. *Estuaries* 27, 861-866.

Coco, G., and Murray, A.B., 2007. Patterns in the sand: from forcing templates to self-organization, *Geomorphology*, 91(3-4), 271-290.

- Colombini, M., Stocchino, A., 2008. Finite-amplitude river dunes. *J. Fluid Mech.*, 611, 283–306, doi :10.1017/s0022112008002814.
- Dalrymple, R.W., Rhodes, R.N., 1995. Estuarine dunes and bars, in: *Geomorphology and Sedimentology of Estuaries. Developments in Sedimentology*. pp. 359–422.
- Ewing, RC, Kocurek, G, Lake, L.W., 2006. Pattern analysis of dune - field parameters. *Earth Surf. Process. Landf.*, 31: 1176-1191.
- Ferret, Y., Le Bot, S., Tessier, B., Garlan, T., Lafite, R., 2010. Migration and internal architecture of marine dunes in the eastern English Channel over 14- and 56-year intervals: The influence of tides and decennial storms. *Earth Surf Process Landf*, 35 (12), 1480–1493.
- Flemming, B., W., 1980. Sand transport and bedform patterns on the continental shelf between Durban and Port Elizabeth (Southeast African continental margin). *Sediment. Geol.* 26, 179–205. doi:10.1016/0037-0738(80)90011-1
- Gonzalez, R., Eberli, G.P., 1997. Sediment transport and bedforms in a carbonate tidal inlet; Lee Stocking Island, Exumas, Bahamas. *Sedimentology* 44, 1015–1030.
- Hendershot, M.L., Venditti, J.G., Bradley, R. W., Kostaschuk, R.A., Church, M., Allison, M.A, 2018. Crestline bifurcation and dynamics in fluvially-dominated, tidally-influenced flow. *Sedimentology* 65 (7). 2621-2636; <https://doi.org/10.1111/sed.12480>.
- Hoekstra, P., Bell, P., van Santen, P., Roode, N., Levoy, F., Whitehouse, R., 2004. Bedform migration and bedload transport on an intertidal shoal. *Cont. Shelf Res.* 24, 1249–1269.
- Huntley, D.A., Coco, G., Bryan, K.R., Murray, A.B., 2008. Influence of “defects” on sorted bedform dynamics. *Geophys. Res. Lett.* 35. L02601. doi:10.1029/2007GL030512.

Komar, P.D., McDougal, W.G., Marra, J.J., Ruggiero, P., 1999. The rational analysis of setback distances: Applications to the Oregon Coast: *Shore & Beach*, v. 67, p. 41-49.

Knaapen, M., A., F. 2005. Sandwave migration predictor based on shape information. *J. Geophys. Res.*, 110, F04S11, doi:10.1029/2004JF000195.

Kostaschuk, R., Villard, P., Best, J., 2004. Measuring velocity and shear stress over dunes with acoustic Doppler profiler. *J. Hydraul. Eng.* 130, 932–936.

Labat, D., 2005. Recent advances in wavelet analyses: Part 4. A review of concepts. *J. Hydrol.*, 314 (1–4), 275–288. <http://dx.doi.org/10.1016/j.jhydrol.2005.04.003>.

Larcombe, P., Jago, C.F., 1996. The morphological dynamics of intertidal megaripples in the Mawddach Estuary, North Wales, and the implications for palaeoflow reconstructions. *Sedimentology* 43, 541–559.

Loquet, N., Rybarczyk, H., Elkaim, R., 2006. Echanges de sels nutritifs entre la zone cotiere et un systeme estuarien intertidal : La baie de somme (Manche, France). *Oceanologica Acta*, 23(1), 47–64.

Massei, N., Dieppois, B., Hamlich, D.M., Lavers, D.A., Fossa, M., Laignel, B., Debret, M., 2017. Multi time-scale hydro-climate dynamics of a regional watershed and links to large-scale atmo-spheric circulation: Application to the Seine river catchment, France. *J. Hydrol.* 546, 262—275, <http://dx.doi.org/10.1016/j.jhydrol.2017.01.008>.

Masselink, G., Cointre, L., Williams, J., Gehrels, R., Blake, W., 2009. Tide-driven dune migration and sediment transport on an intertidal shoal in a shallow estuary in Devon, UK. *Mar. Geol* 262(1):82-95, doi:10.1016/j.margeo.2009.03.009.

Michel C., Le Bot S., Druine F., Costa S., Levoy F., Dubrulle-Brunaud C., Lafite R., 2017. Stages of sedimentary infilling in a hypertidal bay using a combination of sedimentological,

morphological and dynamic criteria (Bay of Somme, France). *Journal of Maps*, 13:2, 858-865 (DOI: 10.1080/17445647.2017.1389663).

Parsons, D.R., Best, J.L., Orfeo, O., Hardy, R.J., Kostaschuk, R., Lane, S.N., 2005. Morphology and flow fields of three-dimensional dunes, Río Paraná, Argentina: Results from simultaneous multibeam echo sounding and acoustic Doppler current profiling. *J. Geophys. Res. Earth Surf.*, 110, F04S03, DOI: 10.1029/2004JF000231

Parteli, E.J.R., Kroy, K., Tsoar, H., Andrade, J.S., Poschel, T., 2014. Morphodynamic modeling of aeolian dunes: Review and future plans. *Eur. Phys. J.*, 223, 2269–2283 (2014), DOI: 10.1140/epjst/e2014-02263-2

Pattanapol, W., Wakes, S., Hilton, M., Dickinson, K., 2008. Modelling of surface roughness for flow over a complex vegetated surface. *International Journal of Mathematical, Physical and Engineering Sciences*, 2(1), 18-26.

Priest, G.R., Allan, J.C., 2004. Evaluation of coastal erosion hazard zones along dune and bluff backed shorelines in Lincoln County, Oregon: Cascade Head to Seal Rock, Technical Report to Lincoln County (Oregon Department of Geology and Mineral Industries, Open-File Report O-04-09).

Soulsby, R.L., 1997. *Dynamic of marine sands*. Thomas Telford publication, UK. 249.

Soulsby, R.L., Whitehouse, R.J.S., 2005. Prediction of Ripple Properties in Shelf Seas - Mark Predictor (Report TR 150).

Soulsby, R.L., Whitehouse, R.J.S., Marten, K.V., 2012. Prediction of time-evolving sand ripples in shelf seas. *Cont. Shelf Res.* 38, 47–62. doi:10.1016/j.csr.2012.02.016

Southard, J.B., Boguchwal, L.A., 1990. Bed configurations in steady unidirectional water

flows. Part 2. Synthesis of flume data. *J. Sediment. Petrol*, 60, 658–679

Stockdon, H.F., Holman, R.A., Howd, P.A., Sallenger, A.H., 2006. Empirical parameterization of setup, swash, and runup: *Coast. Eng.*, v. 53, no. 7, p. 573-588. <https://doi.org/10.1016/j.coastaleng.2005.12.005>

Terwindt, J.H.J., Brouwer, M.J.N., 1986. The behaviour of intertidal sandwaves during neap-spring tide cycles and the relevance for palaeoflow reconstructions. *Sedimentology* 33, 1–31. <https://doi.org/10.1111/j.1365-3091.1986.tb00742.x>.

Traykovski, P., Hay, A.E., Irish, J.D., Lynch, J.F., 1999. Geometry, migration, and evolution of wave orbital ripples at LEO-15. *J. Geophys. Res.* 104, 1505–1524. doi:10.1029/1998JC900026

Turki, I., Laignel, B., Chevalier, L., Costa, S., Mossei, N., 2015. Coastal sea level changes in the southeastern side of the English channel: potentialities for future SWOT applicability. *IEEE J. Sel. Top. Appl. Earth Obs. Remote Sens.* 8 (4), 1564—1569, <http://dx.doi.org/10.1109/JSTARS.2015.2419613>.

Turki, I., Medina, R., Gonzalez, M., Coco, G., 2013. Natural variability of shoreline position: observations at three pocket beaches. *Mar Geol* 338:76–89. doi: 10.1016/j.margeo.2012.10.007.

Vah, M., Jarno, A., Le Bot, S., Ferret, Y., Marin, F., 2020. Bedload transport and bedforms migration under sand supply limitation. *Environ Fluid Mech*, 20, 1031–1052. DOI: 10.1007/s10652-020-09738-6. Doi: <https://doi.org/10.1007/s10652-020-09738-6>.

Venditti, J. G., Church, M., Bennett, S. J., 2005. Morphodynamics of small-scale superimposed sand waves over migrating dune bed forms, *Water Resour. Res.*, 41, W10423, doi:10.1029/2004WR003461.

- Villard, P.V., Church, M., 2005. Bar and dune development during a freshet: Fraser River Estuary, British Columbia, Canada. *Sedimentology*, 52, 737–756.
- Wakes, S.J., T. Maegli, K.J.M. Dickinson and M.J. Hilton, 2010. Numerical modelling of wind flow over a complex geometry. *Environ. Modell. Softw.*, 25(2), 237-247.
- Werner, B.T., 1999. Complexity in natural landform patterns. *Science*, 284, doi: 10.1126/science.284.5411.102.
- Werner, B.T., Kocurek, G., 1997. Bedform dynamics: Does the tail wag the dog?, *Geology*, 25, 771– 774.
- Whitmeyer, S.J., FitzGerald, D.M., 2008. Episodic dynamics of a sandwave field. *Mar. Geol.*, 252, 24–37.
- Wilbers, A.W.E., 2004. The development and hydraulic roughness of subaqueous dunes. Published PhD-thesis, The Royal Dutch Geographical Society (Utrecht, the Netherlands) 323-227.
- Wilbers, A.W.E., ten Brinke, W.B.M., 2003. The response of subaqueous dunes to floods in sand and gravel bed reaches of the Dutch Rhine. *Sedimentology*, 50: 1013-1034.
- Williams, J. J., Bell, P. B., Thorne, P. D., 2005. Unifying large and small wave-generated ripples, *J. Geophys. Res.* 110, C02008, doi:10.1029/2004JC002513.
- Williams, J.J., Carling, P.A., Bell, P.S., 2006. Dynamics of intertidal gravel dunes. *J. Geophys. Res. Oceans* 111, C06035.
- Zhou, J., Wu, Z., Zhao, D., Guan, W., Zhu, C., Flemming, B., 2020. Giant sand waves on the Taiwan Banks, southern Taiwan Strait: Distribution, morphometric relationships, and hydrologic influence factors in a tide-dominated environment. *Marine Geology*, 427, 106238.  
<https://doi.org/10.1016/j.margeo.2020.106238>

## Lists of Symbols

Definition	Symbol	Dimension	Unit
Immersed weight sediment transport	$I_t$	$lt^3$	$ms^3$
Total, suspended and bedload sediment transport rate	$q_b, q_s, q_b$	$l^2t^{-1}$	$m^2s^{-1}$
Water, sediment volumic mass	$\rho, \rho_s$	$ml^{-3}$	$kgm^{-3}$
Friction coefficient	$C_f$	no unity	no unity
Bedload, suspended efficiency factor	$\epsilon_b, \epsilon_s$	no unity	no unity
internal angle of friction	$\phi$		radian
local bed slope	$\beta$		radian
Sediment fall velocity	$w_s$	$lt^{-1}$	$ms^{-1}$
velocity	$v$		
unit vector	$i$		
Sediment porosity	$p$	no unity	no unity
gravity	$g$	$lt^{-2}$	$ms^{-2}$
Long-shore velocity at sea-surface and 1 m above the bed	$U_s, U_b$		
Cross-shore velocity at sea-surface and 1 m above the bed	$V_s, V_b$		
Angle between waves and current at the sea-surface and 1 m above the bottom	$\alpha_s, \alpha_b$		
Wave angle	$\theta$		radian
Dune angle	$\gamma_b$		radian
Total, cross, long-dune migration velocity	$V, V_x, V_y$	$lt^{-1}$	$ms^{-1}$
Total, cross, long-dune migration distance	$M, M_x, M_y$	l	m
Instantaneous long- and cross-dune sediment transport	$q_{ld}$ and $q_{cd}$	$l^2t^{-1}$	$m^2\text{hour}^{-1}$
Averaged long- and cross-dune sediment	$Q_{ld}$ and $Q_{cd}$	$l^2t^{-1}$	$m^2\text{survey}^{-1}$

transport			
Cross-dune and long-dune energy flux	$EF_{cd}$ and $EF_{ld}$	Energie/meter .time	J/m.s
Cross-shore and long-shore energy flux	$EF_{csh}$ and $EF_{lsh}$	Energie/meter .time	J/m.s
Wave length of dunes	$\lambda_d$	l	m

Journal Pre-proof

Editor of Marine Geology

22/09/2020

Dear Editor

**I would like to submit the manuscript entitled ‘Morphodynamics of intertidal dune field in a mixed wave-tide environment: case of Baie de Somme in Eastern English Channel’** by Imen TURKI, Sophie Le Bot, Nicolas Lecoq, Hassan Shafiei, Julien Deloffre, Charlotte Michel, Arnaud Hequette, Vincent SIPKA, Robert Lafite to be considered for publications as an original article in the journal of Marine Geology.

This research investigates the morphological changes of dunes and their migration in relation with the nearshore driving forces. We believe these findings will be of interest to the readers of your journal.

We declare that this research is original in its methodological approach and also the scientific results, not investigated by previous works in this task. This research has not been published before and is not currently considering for publication elsewhere.

The substantial contribution of all co-authors in the present work, combining a series of different approaches, can be summarized follow:

- 1- Field measurements: Sophie Le Bot, Julien Deloffre, Charlotte Michel, Robert Lafite, Arnaud Hequette, Vincent SIPKA
- 2- Analysis: Imen Turki, Nicolas Lecoq, Sophie Le bot, Julien Deloffre, Hassan Shafiei
- 3- Writing-Discussion: Imen Turki, Sophie Le Bot, Nicolas Lecoq, Julien Deloffre, Hassan Shafiei, Robert Lafite

We know of no conflict of interest related to this research and no financial support influencing its outcome. As corresponding author, I confirm that the manuscript has been read and approved for submission by different authors.

Best regards

Imen TURKI

1. Morphodynamics of intertidal dunes in a mixed wave-tide environment is complex
2. Morphological dune response involves different defects of multiple length scales
3. The dune sinuosity is developed under high wave obliquity
4. Dune migration is related to their orientation and the wave-tide conditions

Journal Pre-proof

MORPHODYNAMICS	HIGH ENERGY EPISODES	LOW ENERGY EPISODES
Hydrodynamic conditions	<p>Energy Episodes: E2 and E3 spring tides (T7 – T18)</p> <p>Maximum Tidal Currents: 0.65 m/s (near sea-bed) and 1.2 m/s (surface)</p> <p>Maximum Wave Height: 2 m</p> <p><math>E_{cd} &gt; 1000 \text{ J/m.s}</math></p> <p><math>E_{ld} &gt; 2000 \text{ J/m.s}</math></p>	<p>Energy Episodes: E1 and E4 neap tides (T1 – T6)</p> <p>Maximum Tidal Currents: 0.15 m/s (near sea-bed) and 0.15 m/s (surface)</p> <p>Maximum Wave Height: 0.5 m</p> <p><math>E_{cd} &lt; 1000 \text{ J/m.s}</math></p> <p><math>E_{ld} &lt; 1000 \text{ J/m.s}</math></p>
Wave obliquity : $ \theta $	45° and 55°	0° and 15°
Defects	Sinuosity of dune crestline $\sim 25 \text{ m}$ wavelength	Small Superimposed Large Superimposed
Dune angle: $ \gamma_d $	30° and 45°	15° and 30°
Long-dune migration $V_{ld}$ ( $V_y$ )	<p>Max Positive (<math>+V_{ld}</math>): + 0.25 m/day</p> <p>Max negative Migration (<math>-V_{ld}</math>): - 0.05 m/day</p> <p><math>\sim 35\%</math> of the total dune migration.</p>	<p>Max Positive (<math>+V_{ld}</math>): + 0.15 m/day</p> <p>Max negative Migration (<math>-V_{ld}</math>): - 0.05 m/day</p> <p><math>\sim 65\%</math> of the total dune migration.</p>
Cross-dune migration $V_{cd}$ ( $V_x$ )	<p>Max Clockwise (<math>+V_{cd}</math>): + 0.45 m/day</p> <p>Max Counter-clockwise Migration (<math>-V_{cd}</math>): - 0.45 m/day</p> <p>More than 65% of the total dune migration.</p>	<p>Max Clockwise (<math>+V_{cd}</math>): + 0.15 m/day</p> <p>Max Counter-clockwise Migration (<math>-V_{cd}</math>): - 0.15 m/day</p> <p><math>\sim 32\%</math> of the total dune migration.</p>